A Study of Quantitative Design Method of Adaptive Current Control System with Armature Resistance Identification Function

Jun-ichi Itoh
Dept. of Electrical, Electronics and Information Engineering
Nagaoka University of Technology
Nagaoka Niigata, Japan
itoh@vos.nagaokaut.ac.jp

Yuki Nakajima
Dept. of Electrical, Electronics and Information Engineering
Nagaoka University of Technology
Nagaoka Niigata, Japan
nyuuki@stn.nagoakaut.ac.jp

Abstract— **This paper clarified quantitative design method of adaptive current control system with armature resistance identification function. Additionally, it was proved in this design method that response error occurs between design and actual responses. However, it was confirmed from analysis that the error does not depend on motor parameters. As a result, the response error can be compensated by adding margin into the design value.**

Keywords- IPMSM; armature resistance identification; adaptive current control; design method

I. INTRODUCTION

Recently, the sensorless vector control has been attracted attention intensely. The sensorless vector control is a low cost structure but achieves high reliability in the motor drive system. Therefore, many sensorless vector control methods have been proposed and studied [1-6].

In the sensorless vector control, accurate motor parameters are required to achieve high performance because these parameters are needed to estimate magnetic pole position. However, these motor parameters are different from one to another even it is a same type motor. Therefore, a mismatch occurs between the actual armature resistance value and the resistance value which is applied in the sensorless vector control. Additionally, the motor parameters are varied according to the operating condition. For example, the armature resistance value is varied to the temperature. Therefore, if the motor temperature rises, mismatch error will occur. These mismatches will cause a poor control performance especially at low speed. Furthermore, high response resistance identification is important in order to stabilize the motor at low speed drive because the error of output voltage caused by the dead-time is able to take equivalent resistance.

Ref. 7 has proposed a speed and armature resistance identification method based on an adaptive full-order observer to solve the problem. However, this method has a problem that the armature resistance identification system is unstable [8]. Furthermore, in case that the position estimation method based on a minimum order of observer is used, a method to identify the armature resistance is required separately because the observer cannot be added with additional armature resistance identifier into the system [9].

In order to solve these problems, an adaptive current control system with armature resistance identification function was suggested [10]. This method is a simple configuration similar to PI current controller. Stability of this method has been ensured by Lyapunov stability theory. Additionally, this system is decoupled with the position estimation system; each identification system is independent to another. Therefore, this method is possible to combine with a position estimation method.

However, the design procedure for this method has not been discussed. In this method, clarification of the design method is important because this method includes the current control system. Additionally, in case where the application has an unstable load such as air conditioner or waving machine, the identification system needs to regulate the responses quick and accurate because the identification operation uses current control error. In another word, when current value converges to command value, identification value converges the actual value. Furthermore, high response identification is needed in order to obtain high accuracy identification function because resistance values are varied by equivalent resistance due to the dead-time.

In this paper, a quantitative design method of the adaptive current control system features to identify armature resistance is discussed. The parameter design of this system needs to consider the response of the current control system because the identification system and the current controller are coupled. This paper is organized as follows: firstly, the adaptive current control system is simplified by linearization to derive the transfer function of a standard form to a second-order system. As a result, design equations of the current control system are derived. Secondly, the parameters that cause the error between design value and actual response are studied. From the result, it is clarified that the error is independent from the motor

parameters. Finally, the accuracy of this design method is confirmed by simulation and experimental results. In the simulation, step response and operation with load oscillation are confirmed. In the experimentation, the step response is confirmed by using a 1.5kW IPMSM and a 2-level inverter.

II. A Quantitative Design Method Of An Adaptive Current Control System

A. Adaptive Current Control System Features Identify Functions With Armature Resistance

Figure 1 shows a block diagram of the adaptive current control system, where K_d and K_q are the proportional gain, g is the adaptive gain, i_d* and i_q* are the dq-axis current command value, i_d and i_q are the dq-axis current detection value, e_{id} and e_{iq} are the current control error, v_d* and v_q* are the dq-axis voltage command value, v_{Rq} and v_{Rd} are the compensated voltage value of voltage drop in armature resistance, ω_m is the angular velocity of the motor, and K_E is the back electromotive force of the motor. This control method identifies the armature resistance value by the use of the current control error.

A voltage control equation of the adaptive current control system is given by (1).

$$\begin{bmatrix} v_d^* \\ v_q^* \end{bmatrix} = \begin{bmatrix} \hat{R} & -\omega_{re} L_q \\ \omega_{re} L_d & \hat{R} \end{bmatrix} \begin{bmatrix} i_d \\ i_q \end{bmatrix} + \begin{bmatrix} K_d & 0 \\ 0 & K_q \end{bmatrix} \begin{bmatrix} e_{id} \\ e_{iq} \end{bmatrix} + \begin{bmatrix} 0 \\ \omega_{rm} K_E \end{bmatrix} \quad (1)$$

where R_a is the armature resistance value, $\hat{R}$ is armature resistance identification value, and L_d and L_q are the dq-axis synchronous inductance. This control system consists of three systems. First is the compensation system for armature resistance and coupling term as shown in the first term of (1). Second is the proportional control system as shown in the second term of (1). Third is the compensation system of back electromotive force as shown in the third term of (1). In addition, the equation to identify the armature resistance is given by (2).

$$\hat{R} = g \int \left(i_d e_{id} + i_q e_{iq} \right) dt \quad (2)$$

Equation (2) is derived by Lyapunov stability theory. This control system ensures the system stability as long as the condition of (2) is satisfied.

B. Quantitative Design Method of Adaptive Current Control System

Figure 2 shows the control block diagram that linearized the nonlinear term of figure 1, where, i_{qs} is the q-axis current steady state value, $F(s)$ is the command filter which transform the transfer function into a second order system. First of all, i_d=0 control is supposed to ignore in the coupling term between d and q axis as shown in Figure 1. Second, the nonlinear term is linearized. v_{Rq} as shown in Fig.2(a) is given by (3).

$$v_{Rq} = i_q \frac{g}{s} \left(i_q e_{iq} \right) \quad (3)$$

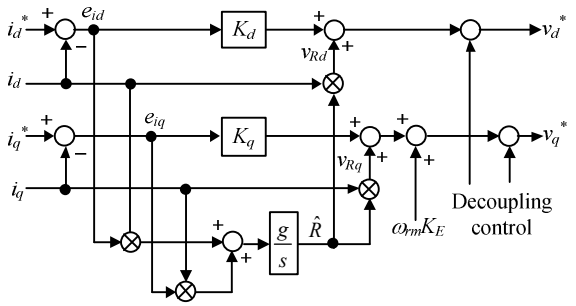

Fig.1 Adaptive current control system.

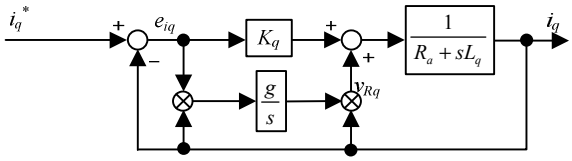

(a) i_d=0 model.

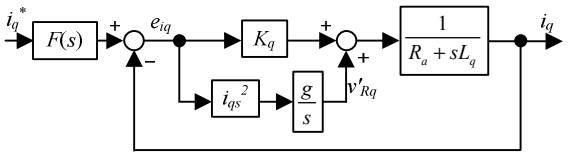

(b) Linearization model.

Fig.2 Linier approximated control block diagram

Equation (3) is a nonlinear equation because there is a multiplication between some variables such as i_q and e_{iq} in this equation. Here, equation (3) is linearized on the supposition that d axis current is nearly a steady state. When (3) is separated into the steady term and ripple term, v_{Rq} is obtained by (4).

$$v_{Rq} = \left(i_{qs} + \Delta i_q \right) \frac{g}{s} \left(i_{qs} e_{iqs} + \Delta i_q e_{iqs} + i_{qs} \Delta e_{iq} + \Delta i_q \Delta e_{iq} \right) \quad (4)$$

where, i_{qs} and e_{iqs} are the steady term, Δi_q and Δe_{iq} are the ripple term. The product of the ripple components Δi_q and Δe_{iq} can be neglected because the value is small. In addition, Δi_q equals to zero when the q-axis current is controlled to constant. Then, linearized v_{Rq} (=v_{Rq}') is obtained by (5).

$$v_{Rq}' = i_{qs} \frac{g}{s} \left(i_{qs} e_{iq} \right) \quad (5)$$

Equation (5) is a linear equation because the i_{qs} is a constant value.

Finally, the command value filter given by (6) is added so that it transforms into a second order system (Fig.2(b)).

$$F(s)=\frac{1}{\frac{K_q}{{i_{qs}}^2 g}s+1} \tag{6}$$

From figure 2(b), transfer function $G(s)$ is obtained by (7).

$$G(s)=\frac{{i_{qs}}^2 g}{L_q s^2+s(R_a+K_q)+{i_{qs}}^2 g} \tag{7}$$

Here, the variables of (7) is compared with the variables in the transfer function of second order system $G'(s)$ given by (8).

$$G'(s)=\frac{{\omega_n}^2}{s^2+2\zeta\omega_n s+{\omega_n}^2} \tag{8}$$

As the result, the proportional gain K_q and adaptive gain g can be obtained by (9) and (10) respectively.

$$K_q = 2\zeta\omega_n L_q - R_a \tag{9}$$

$$g=\frac{{\omega_n}^2 L_q}{{i_{qs}}^2} \tag{10}$$

With any ω_n and ζ value, K_q and g are calculated by (9) and (10). Therefore, it is possible to design any response waveform on this control system.

III. Mathematical Analysis Of The Error Occurring By Linearization

A. Response Error Occurring By Linearization

This design method uses linearization to derive the transfer function. Therefore, the block diagram used to derive design the equation is technically different from the actual current control system. The difference becomes larger when the state of current control system is differed from steady state, which is precondition of linearization. This factor refers that current response waveform becomes different from design value when large variation input occurs on the current command. Therefore, a mathematical method is used to analyze the difference between the actual current and block diagram value, to clarify the parameters depend on the response error.

B. Mathematical Analysis of the Errors

Figure 3 shows the linearization model added with error terms. The error equation is derived as following.

From the comparison between (3) and (5), the relationship between v_{Rq} and v_{Rq}' is obtained as (11).

$$v_{Rq}=\left(1+\frac{\Delta i_q}{i_{qs}}\right)\left(v_{Rq}'+i_{qs}\frac{g}{s}\left(\Delta i_q \Delta e_{iq}\right)\right) \tag{11}$$

From (11), it can be confirmed that the added error and proportional error are including the compensated voltage of voltage drop which is caused by the armature resistance.

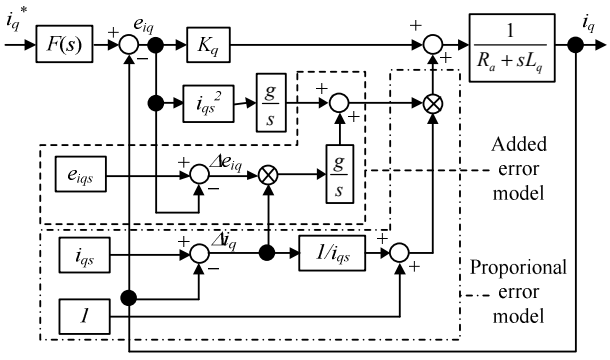

Fig.3 Linear approximated control block diagram with linear approximation error model.

Table.1 Motor Parameters used in simulations.

(a) 800W SPMSM.

Motor Power	800W
Rated Current	8.2A
Rated Speed	2000rpm
Number of Poles	4poles
Winding Resistance	0.425Ω
d-axis inductance	3.78mH
q-axis inductance	3.78mH
Interlinkage magnetic flux	0.233V・s/rad

(b) 750W IPMSM.

Motor Power	750W
Rated Current	4.67A
Rated Speed	1800rpm
Number of Poles	6poles
Winding Resistance	1.98Ω
d-axis inductance	26.6mH
q-axis inductance	57.0mH
Interlinkage magnetic flux	0.284V・s/rad

(c) 3.7kW IPMSM.

Motor Power	3.7kW
Rated Current	19.2A
Rated Speed	1800rpm
Number of Poles	6poles
Winding Resistance	0.693Ω
d-axis inductance	6.2mH
q-axis inductance	15.3mH
Interlinkage magnetic flux	0.330V・s/rad

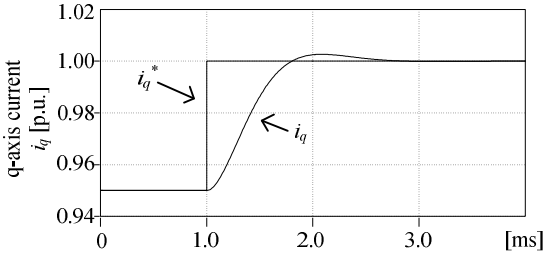

Fig.4 Step response waveform.

Here, equation (11) does not include the motor parameters. Therefore, the occurred error is not depending on the motor

parameters. In addition, the terms for the error units are infinite. As a result, the error is not depending on the rated value of the either.

Based on the above equations, it can be assumed that the response error occurring at the linearization is independent to the motor.

IV. Simulation Results

In this section, simulation results are provided to confirm the step response waveform of the q-axis current. Table 1 shows the simulation conditions. These three motors are different in types of motor and rated power.

A. Accuracy Design in the Proposed Design Method

Figure 4 shows the step response of the q-axis current waveform when the q-axis command value is controlled from 0.95 p.u. to 1.00 p.u.. The motor shown in Table 1(a) is used in this simulation result. In addition, i_{qs} is 1.00p.u. and the load is a constant speed at 0 p.u.. Moreover, the control system is designed as ζ is 0.7 and ω_n is 4000rad/s by using (9) and (10). From figure 4, it is confirmed that the step responses of the q-axis current waveform follows accurately to the step response waveform of the second order system. Furthermore, based on the overshoot waveform and the time to reach peak value (peak of overshoot), these can calculate that ζ is 0.68 and ω_n is 3969 rad/s. Comparing to the design value, the error ratio is approximately -0.8%.

Figure 5 shows a comparison on the step response of q-axis current command with change in the step width operating under a different angular frequency. Here, the ω_{n_cal} is the calculation value of the ω_n from the response waveform, and the ω_{n_des} is the design value of the ωn. From figure 5, it is confirmed that the error between the ω_{n_cal} and the ω_{n_des} becomes larger when the step width of the q-axis current command value becomes larger. This phenomenon agrees with the supposition in the chapter III.B. Thus, the response error becomes larger when the state of the current control system is differed from the steady state because the linearization method assumes the current is nearly to steady state, $i_q = i_{qs}$. Furthermore, the result shows the trend of error is constant with the natural angular frequency

B. Analysis of the response error occurring by the linearization

Figure 6 shows the comparison on the step response of q-axis current command between the block diagram figure 1 and figure 3. Here, i_q* is varied from 0.1 p.u. to 1.0 p.u.. In addition, i_{qs} is 1.0p.u. and control system is designed as ζ=0.7 , ω_n=8000rad/s. Furthermore, in figure 6, i_{q_lin} is the step response waveform of the linearization model (Fig.2(b)), and $i_{q\_lin+err}$ is the step response waveform of the block diagram that added with the error term (Fig.4).

When i_d=0 control is used, the actual current response waveform obtained from the block diagram (Fig.1) is differed from the current response waveform obtained from linearized block diagram (Fig.2(b)). Here, these are confirmed that ζ=0.70 and ω_n=8000 rad/s from the overshoot and the time to reach peak of the response waveform. From the above, when the step width of the q-axis current command value is large, it can be confirmed that the actual response waveform becomes different from the designed response.

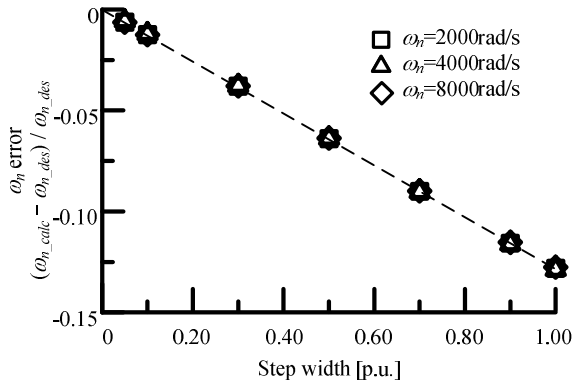

Fig.5 Natural angular frequency between design and simulated value.

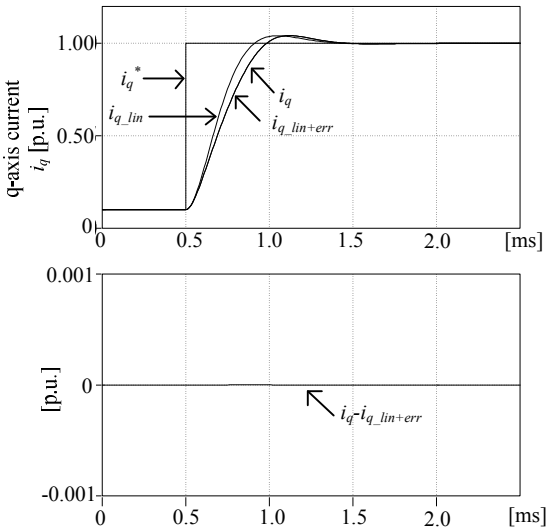

Fig.6 Step response waveform with considering error term model.

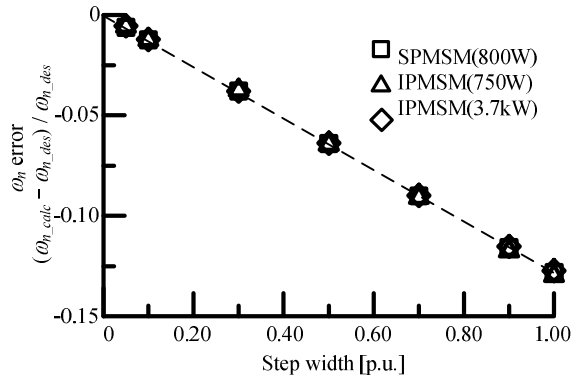

Fig.7 Natural angular frequency error between design and simulated value as three motors.

In addition, the step response waveform as the block diagram of figure 4 is confirmed to the actual current response waveform. Therefore, the cause of the current response error is the added and proportional error term as shown in equation (11).

Figure 7 shows a comparison result with three types of motors. The step width of q-axis current command is varied according to the natural angular frequency. From figure 6, it is confirmed that the error in the natural angular frequency error becomes larger when the step width of the q-axis current command value becomes larger. In addition, the trend of the error remains constant even the motor has changed. Again, it is confirmed that the error in natural angular frequency error rate is not depending on the motor parameters. This result agrees with chapter III.B. Therefore, we can achieve the response by design using the actual design value increased to 1.13 times of required natural angular frequency.

C. Variation of armature resistance identification value with design of current control system

Figure 8 shows the results of armature resistance identification value $\hat{R}$ with and without the proposed design control. Figure 8(a) shows a result that the proposed control is not included, K_q is 3.0 and g is 15.0. On the other hands, Figure 8(b) demonstrates a result that included the proposed control system, the design values are follows ζ is 0.7 and ω_n is 4000rad/s by using (9) and (10), respectively. When the load is fluctuating, q-axis current is changing and $\hat{R}$ becomes different. If the control system is not designed correctly, then the $\hat{R}$ will not converge. In another words, armature resistance value cannot be identified. On the other hands, if the control system is designed correctly, the $\hat{R}$ can be converged and the armature resistance value can be identified. Therefore, it can clarify that the identification system is necessary in order to design the system correctly.

V. EXPERIMENTAL RESULTS

Figure 9 shows the experimental schematic. In the experimental setup, the AC source is connected to the diode rectifier stage as an input power, and an IPM motor is connected to the inverter stage. Furthermore, an induction motor is connected to the IPM motor stage as a load. Table 2 shows the motor parameter using in the experiment. The motor is 1.5 kW and 2000rpm.

A. Response Error Occurring By Linearization

Figure 10 shows the step response of q-axis current waveform when the i_q^* is varied from 0.5p.u. to 0.7p.u.. In this case, ζ=0.7, and ω_n is varied from =1000 rad/s, 2000 rad/s, and 4000 rad/s. Here, i_d=0 control is used, i_{qs} is 1.0p.u.. In addition, the load was a constant speed at 0 p.u.. From figure 10, it is confirmed that the i_d is controlled to nearly 0 p.u.. Additionally, it is confirmed that the step response waveform of i_q corresponds to the step response waveform of the second order system even the ω_n is changed. Furthermore, the setting time of i_q becomes half when the design value of natural angular frequency is double. From the above, the validity of the clarified design method in the chapter II can be confirmed.

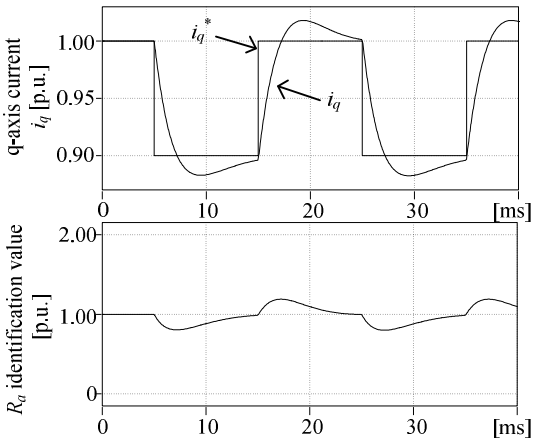

(a) K_q=3.0 g=15.0 (not using command filter)

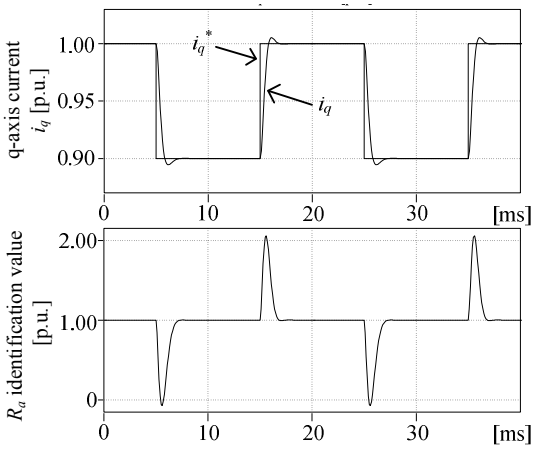

(b) K_q=20.7 g=899.5(ζ=0.7 ω_n=4000rad/s).

Fig.8 Response of load oscillation

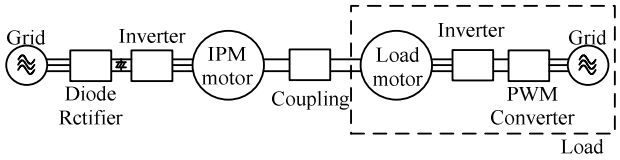

Fig.9 Experimental system.

Table.2 Motor Parameters used in experimentations.

Motor Power	1.5kW
Rated Current	8.6A
Rated Speed	2000rpm
Number of Poles	4poles
Winding Resistance	0.783Ω
Synchronous reactance	11.5mH
Interlinkage magnetic flux	0.308V･s/rad

B. Analysis of the response error occurring by the linearization

Table 3 shows the natural angular frequency calculated from the overshoot and time to reach peak of overshoot based on figure 10. From table 3, the error rate of natural angular frequency is lesser than 10%, which demonstrate a high

accuracy in the designed system. However, the error rates of natural angular frequency are varied with the design value of natural angular frequency. In considered to this subject, the influence of discretization in the controller is investigated.

Figure 11 shows the comparison results of the natural angular frequency between simulation and experimental results. Note that the simulation result calculated from simulator, which the simulation condition is confirmed similar to the experimental condition. The simulation results are shown in continuous and discrete system for each design. From figure 11, the trend of natural angular frequency obtained by experiment and simulation are nearly matched. In addition, the natural angular frequency errors occur between the design value and the simulation result in the continuous system is approximately at 25% difference. This trend is similar to the error of natural angular frequency as shown in figure 5. Furthermore, when the controller is discretized, variable of the actual natural angular frequency is confirmed. Accordingly, it is considered that the divergence between experimental result and analysis value is caused by the discretization.

Table 4 shows finite values of the resistance identification. For the experimental result, it is confirmed that resistance identification value is converged at approximately 1.3p.u.. This result shows that the true resistance value during experimentation is around 1.3 times higher than the nominal resistance value. Here, the resistance value measured immediately after the experimentation is around 1.2 times higher than the nominal resistance value. The cause of difference between the measured value and the nominal value of armature resistance is temperature which is the heat caused by the current.

Figure 12 shows the comparison result on a 10% setting time of resistance identification value between the simulation and experimental results. Here, the simulation result is obtained by the discretization model. From figure 11, it is confirmed that the setting time of identification value is well matched with the simulation result. This result shows that the time to converge the resistance identification value can set to be an arbitrarily.

VI. CONCLUSION

In this paper, the quantitative design method of the adaptive current control system functions to identify armature resistance has discussed. Firstly, the quantitative design method of the adaptive current control system was clarified. Secondly, the cause of the error in the design was analyzed. Finally, the following shows the conclusion based on the simulation and experimental results.

1) When the current is nearly to steady state, it was confirmed that the error ratio of natural angular frequency is approximately -0.8% comparing to the design value.

2) The error of natural angular frequency occurs depending on the step width in the linearization. However, this error is possible to compensate because this error is not depending on the motor parameters.

3) The validity of the design method has confirmed in simulation. Additionally, it was clarified that the natural angular frequency is not depending on the motor parameter.

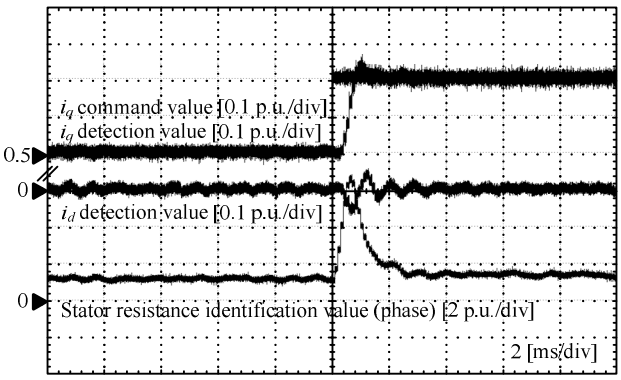

(a) ω_n=4000rad/s ζ=0.7

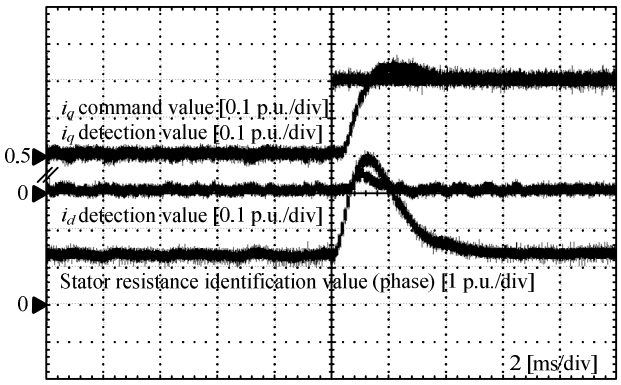

(b) ω_n=2000rad/s ζ=0.7

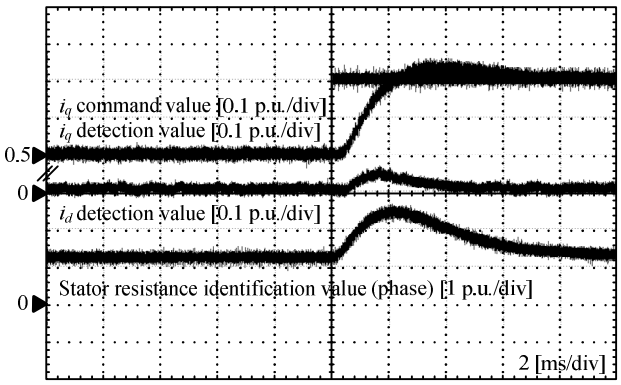

(c) ω_n=1000rad/s ζ=0.7

Fig.10 Step response waveform as the experimentation.

Table.3 natural angular frequency calculated from experimental waveform.

Design value	Calculated value	Error
4000rad/s	3848rad/s	-3.8%
2000rad/s	1885rad/s	-5.7%
1000rad/s	1001rad/s	0.1%

4) From the experimental results, it was confirmed that the step response waveform of the i_q corresponds to the step response waveform of the standard form of the second order system. In addition, the error of natural angular frequency is lesser than 10%.

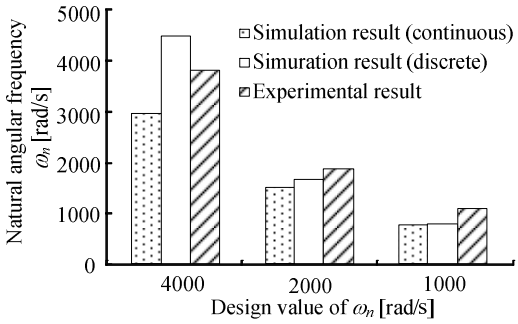

Fig. 11 Comparison experimental results with simulation results.

Table.4 Armature resistance identification value obtained by experiment.

Design value	Resistance identification value
4000rad/s	1.37p.u.
2000rad/s	1.26p.u.
1000rad/s	1.32p.u.

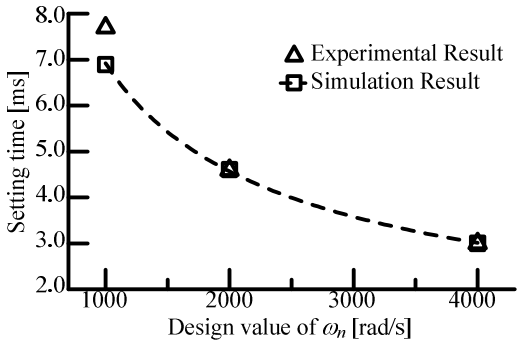

Fig.12 Setting time of armature resistance identification value.

REFERENCES

[1] M. J. Corley, and R. D. Lorenz : "Rotor Position and Velocity Estimation for a Salient-Pole Permanent Magnet Synchronous Machine at Standstill and High Speeds", IEEE Transactions on Industry Applications Vol. 34, No. 4, pp784-789 (1998)

[2] S.Morimoto, K.Kawamoto, and Y.Takeda : "Position and Speed Sensorless Control for IPMSM Based on Estimation of Position Error", T.IEEJapan Vol.122, No.7, pp.722-729 (2002)

[3] S.Ichikawa, Z.Chen, M.Tomita, S.Doki, and S.Okuma : "Sensorless Controls of Salient-Pole Permanent Magnet Synchronous Motors Using Extended Electromotive Force Models", T.IEEJapan Vol.122, No.12, pp.1088-1096 (2002)

[4] S.Ogasawara, H.Kurokawa, and H.Akagi : "A Position-Sensorless IPM Motor Drive System Using a Detection Circuit of Current Variations", T.IEEJapan Vol.123, No.6, pp.667-674 (2003)

[5] K.Shingai, and T. Noguchi : "Spatial Harmonics Based Mechanical Sensorless Control of Concentrated Wound IPM Motor", Proc. of IEEJapan IAS 2004, pp.I-343-346(2004)

[6] M,Tomita, M.Hasegawa, and K.Matsui : "Design Method of Full-Order Extended Electromotive Force Observer for Sensorless Control of IPMSM", Proc. of IEEJapan IAS 2009, pp.I-339-342 (2009)

[7] T.Hamajima, M.Hasegawa, S.Doki, and S.Okuma : "Sensorless Vector Control of Induction Motor Stabilized at the Whole Region with Speed and Stator Resistance Identification based on Augmented Error", T.IEEJapan, Vol.124, No.8, pp.750-759 (2004)

[8] T.Tateyama, T.Ohba, and H.Kubota : "Speed Estimation and Stator Resistance Estimation of Induction Machines Using Estimation Error Index and Stability Consideration", T.IEEJapan, Vol.129, No.8, pp.794-801 (2009)

[9] S.Ichikawa, M.Tomita, S.Doki, and S.Okuma : "Sensorless Control of Permanent-Magnet Synchronous Motors Using Online Parameter Identification Based on System Identification Theory", IEEE Trans. on Industrial Electronics, Vol.53, No.2, pp.363-372 (2006)

[10] K.Kojima, M.Hasegawa, K.Matsui :"Resistance Identification Based on Adaptive Current Control System and Performance Improvement in Low Speed Region for IPMSM Position Sensorless Control" Proc. of IEEJapan IAS 2010, pp.I-303-304 (2010)